Highlights

Laser micromachined 3D glass photonics platform demonstrated by temperature compensated strain sensor

Viktor Geudens, Shahryar Nategh, Geert Van Steenberge, Jan Belis, Jeroen Missinne

- Full 3D platform for integrated glass photonics
- Versatile laser micromachining with etching capabilities
- Building blocks to easily create complex circuits
- Temperature compensated strain sensor with sensitivities of 10.5 pm $^{\circ}C^{-1}$ and 1.1 pm/$\mu\epsilon$

Laser micromachined 3D glass photonics platform demonstrated by temperature compensated strain sensor

Viktor Geudens[a,*], Shahryar Nategh[a,1], Geert Van Steenberge[a], Jan Belis[b], Jeroen Missinne[a]

[a] *Center for Microsystem Technology (CMST), Ghent University and imec, Technologiepark 126, Zwijnaarde, 9052, Belgium*
[b] *Department of Structural Engineering, Ghent University, Technologiepark 60, Zwijnaarde, 9052, Belgium*

Abstract

A platform for integrated glass solutions with full 3D capabilities based on femtosecond laser micromachining is presented. The design and fabrication of different building blocks, such as optical waveguides, bragg gratings, V-grooves and (freestanding) microstructures are described. The capabilities of the platform are exemplified by designing a temperature compensated strain sensor composed of two Bragg grating sensors, where one Bragg grating sensor is mechanically isolated by means of a cantilever, while the other is embedded in the bulk of the glass. Both Bragg gratings exhibit a similar temperature sensitivity of about 10.5 pm $^{\circ}C^{-1}$. It is proven that the isolated Bragg grating does not experience strain, while the other one does with a sensitivity of 1.1 pm/$\mu\epsilon$; thus allowing temperature compensation. Integrated V-grooves allow for a fully fiber-packaged strain sensing solution, directly applicable in many structural health monitoring applications. The versatility of the platform is further illustrated by the widely varying building blocks.

Keywords:
strain, temperature compensation, Bragg grating, waveguide, monolithic, glass, fused silica, femtosecond laser, FLICE, FLDW, platform

1. Introduction

The most established technology nowadays in glass photonics are optical fibers. In combination with other discrete components, such as splitters, filters, and gratings, they can form complex systems. However, due to their discrete nature, these systems are rather bulky and rely on accurate alignment between all these components. This is a costly and time-consuming procedure, and additionally, several applications benefit from miniaturized implementations. Integration of these components in a single glass substrate is able to overcome these issues. Moreover, integrated glass photonics pushes the miniaturization of optical components to chip-level. Densely combining different functionalities together on chip, where alignment is defined during the fabrication process, reduces the cost, while increasing the manufacturability and performance of complex photonic systems and opens up new application domains.

This effort of component integration on a single glass substrate is ongoing, and has been established by lithographic planar lightwave circuit (PLC) technology. PLCs integrate multiple functionalities on a single substrate, and allow for hybrid integration of for example laser sources. They are heavily used in the field of telecommunications [1].

PLCs can integrate glass based optical waveguides and extend functionalities in certain aspects. However, they are limited mainly by their planar nature [2, 3]. Integrating out-of-plane capabilities in combination with selective etching allows to create complex integrated glass structures that are not possible with PLCs. 3D waveguides and freestanding structures open new possibilities in many areas such as structural health monitoring, and biomedical applications.

In this paper, we present a fabrication platform that allows monolithical integration of nowadays discrete glass components into a single glass chip. The platform extends the functionalities of lithographically fabricated glass PLCs by exhibiting full 3D capabilities and being able to create (freestanding) microstructures.

2. 3D glass photonics platform

The platform is based on femtosecond laser micromachining of fused silica. The basic principle of femtosecond laser direct writing (FLDW) is that ultra-short laser light pulses are focused into the bulk of the transparent substrate. The high intensity field yields nonlinear effects, such as multiphoton absorption. The relaxation transfers the energy to the material, causing a permanent materal change, such as a permanent change in refractive index [4]. Since these nonlinear effects occur only locally in the focal volume, small structures can be created. By translating the focal volume in the bulk of the substrate, arbitrary complex 3D structures can be formed. Since the discovery in 1996 [5], a broad range of functionalities were demonstrated as an integrated glass solution. These components include waveguides, splitters, couplers, Mach-Zehnder interferometers, and even Bragg grating waveguides, the integrated equivalent of fiber Bragg gratings [6, 7, 8, 9, 10, 11].

*Viktor.Geudens@UGent.be

Apart from a permanent change in refractive index, under the right conditions, the laser affected regions exhibit a significantly higher etching speed in a variety of echting solutions such as KOH, (B)HF, and NaOH, compared to non-irradiated material. These high etch selectivities are used in femtosecond laser irradiation followed by chemical etching (FLICE) processes to create 3D structures with high accuracy, small dimensions, and high apect ratios [12, 13]. The main work reported regarding FLICE focuses on the creation of microchannels and microfluidic devices [14, 15]. For the latter, FLDW is combined with static FLICE-structures. However, combining these two technologies into a single MOEMS-like device with freestanding microstructures has been scarcely investigated. These structures increase the flexibility of design, and open up new routes in many application fields. Here, the applications in structural health monitoring are demonstrated by creating a temperature compensated strain sensor.

3. Materials and methods

3.1. Fabrication

In this paper, the aforementioned concept was realized by exploiting the capabilities of femtosecond laser direct writing (FLDW) and femtosecond laser irradiation followed by chemical etching (FLICE) in fused silica glass. This is a two-step process where first all laser irradiation is performed in a single step, and then the substrate is chemically etched.

The laser used is a Satsuma femtosecond laser (Amplitude) followed by a second harmonic generation module, to obtain a lasing wavelength of 515 nm. The pulse repetition rate was fixed to 500 kHz. In the beampath a half-wave plate and quarter-wave plate are inserted in rotation stages, allowing full control of the polarization of the laser light. For all structures that required etching, i.e. the cantilever and V-grooves, the polarization was set to be circular, whereas linear polarization parallel to the writing direction was used for the (Bragg grating) waveguides. Lastly, the laser light is focused in the fused silica substrate with the help of a aspheric lens with NA 0.55 (Newport 5722-A-H). The fused silica substrate is mounted on a vacuum chuck of a motorized XY-stage.

The waveguides were formed using a pulse energy of 310 nJ with a stage translation speed of 0.5 mm s^{-1}. Bragg grating waveguides were created by applying an external modulation of 500 Hz and adjusting the writing speed according to

$$v = \frac{\lambda_B f}{2n_{eff}} \tag{1}$$

where v is the translation speed, λ_B represents the target Bragg wavelength, f is the external modulation frequency, and n_{eff} denotes the effective refractive index. The structures that required etching (i.e. V-grooves and cantilever) were fabricated with a pulse energy of 200 nJ and a writing speed of 10 mm s^{-1} for dimensions along the length of the structures, and 1 mm s^{-1} for the other dimensions. Subsequently, the laser-exposed substrate is chemically etched by submerging it in a 30 w% KOH-solution at an elevated temperature of 85 °C for 3 times 4 h.

3.1.1. Fiber attachement

After having fabricated the sensor, it still requires packaging to interface with the outer world. To facilitate packaging, a V-groove is added in the glass as mentioned before (also see Figure 6). This allows passive alignment, and the fiber is more mechanically stable after fixation in the V-groove. This still has a weak point at the edge of the sample where the bare fiber is sticking out of the V-groove. However, by cleaving the bare fiber to the same length as the V-groove, the glue to fix the fiber will cover the bare fiber and connect to the plastic coating around the fiber; thus making the edge thicker and mechanically stronger. The fibers are glued in an array of V-grooves using UV-curable glue NOA 61 and NOA 63 (Norland Products). The less viscous NOA 61 is first used to fixate the fibers in the V-groove. Next, NOA 63 is applied as extra bonding and encapsulation layer. Adding a top plate on top of the fibers could improve mechanical stability further.

3.2. Characterization

3.2.1. Strain characterization

The strain response of the sensor was investigated by a tensile test, where the force was applied along the length of the Bragg grating waveguides. To allow easy clamping of the sensor and with future applications in mind, the glass sensor was bonded to an aluminium base plate with dogbone shape (see Figure 1) using epoxy glue (Sikadur 30, Sika). This shape is chosen to increase the strain applied to the sensor while limiting the required load. First, both the sensor and the base plate were thoroughly cleaned. Epoxy was applied to the bottom-side of the sensor, which was then brought into contact with the base plate. Finally, the epoxy was cured for a day at an elevated temperature of 35 °C. The bonded sensor is also depicted in Figure 1. As can be seen in the picture, no epoxy is applied to the region underneath the V-grooves to avoid straining the fiber connection. Details are found in the supplementary information. The aluminium base plate is clamped in a universal testing machine (Instron 5982-100kN) after which the load is applied. As a reference, strain gauges (Micro-Measurements) are attached to both the glass sensor and the backside of the base plate.

A stepwise displacement of 35 µm is applied and after each displacement step the sensor response is read out three times with a commercially available FBG-interrogator (FBG-scan 608, FOS&S now FBGS). Transition between displacement was programmed to have a speed of 0.875 µm s^{-1}. The reference strain gauges were read out using VISHAY system 5000 (Micro-Measurements).

3.2.2. Thermal characterization

The sensor was placed in a climate chamber (Vötsch VTS 7040-15) and thermal cycling was performed. The temperature was changed from 10 °C to 120 °C and back to 10 °C with steps of 10 °C and a speed of 5 °C min^{-1}. This cycle was repeated four times. After each temperature change, the temperature was kept constant for 20 min to ensure the temperature was stabilized before the reflection spectrum had been obtained. As a

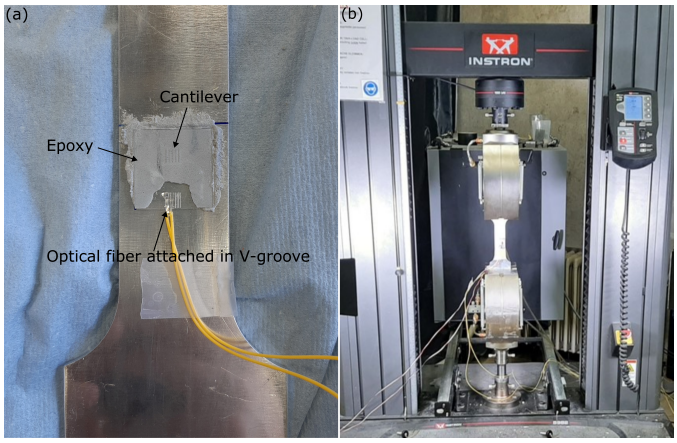

Figure 1: (a) Fused silica sensor substrate bonded to an aluminium base plate for strain characterization. (b) Sensor bonded to aluminum base plate, clamped in the universal testing machine for tensile test.

reference sensor a K-type thermocouple was positioned next to the glass substrate. The reflection spectrum of the sensor was again read out using an FBG-scan 608 interrogator, while the thermocouple was read out using a Pico USB TC-08 controller, both interfaced with a computer.

3.2.3. Data analysis

The bare Bragg grating reflection spectra obtained from the FBG608 during the thermal and strain characterization of the sensor were analyzed and visualized using MATLAB. For more accurate peak detection of the Bragg gratings, a center of gravity algorithm was implemented [16].

3.3. Strain transfer simulation

The simulations to investigate the influence of applying epoxy on the strain transfer from the aluminum base plate to the sensor substrate were performed using COMSOL. The full 3D structure of the base plate and sensor were modeled. The sensor was divided into different sections. Then boundary conditions between the glass substrate and the base plate were changed between *adhesion* and *free* for each section independently. A constant force was applied on the front and back facet of the top side of base plate, while the same facets of the bottom side were fixed. The strain distribution over the sensor substrate was extracted for each of the different settings of boundary conditions.

4. Results and discussion

In the following sections different building blocks are described. Afterwards, a temperature compensated strain sensor realized using these building blocks is presented to showcase the strength and flexibility of this platform.

4.1. Building blocks

4.1.1. Optical waveguides

The most essential building block of integrated photonic circuits, regardless of the technology platform, are waveguides. By changing the fabrication parameters of the laser writing process, the waveguide properties, such as mode field diameter (MFD) and losses, can be optimized for the target applications. The writing speed and pulse energy are swept within the range 0.05-3 mm s^{-1} and 150-420 nJ, respectively. The waveguide losses and MFD were measured for each set of parameters, see Figure 2. For the fabrication of single mode waveguides operating around 1550 nm and interfaced with a single mode fiber (SMF-28), the optimal parameters are a writing speed of 0.5 mm s^{-1} with a pulse energy of 310 nJ. This set of parameters combine a low propagation loss of less than 0.5 dB cm^{-1} with a MFD only slightly higher than 11 µm, which closely matches the 10.4 µm MFD of a SMF-28 at a wavelength of 1550 nm.

Since the MFD can be tuned by optimizing the writing speed and pulse energy, it is possible to fabricate tapers. By accelerating/decelerating and/or increasing/decreasing the pulse energy during the writing, down/up tapering can be achieved. This can be used for mode matching when butt-coupling or for expanding the MFD to achieve a larger lateral alignment tolerance in a connector or during packaging [17].

Splitters and couplers are a valuable part of waveguide structures. They allow for splitting and combining light with arbitrary ratios, and are essential in many interferometers. Both splitters [18], and couplers [19] have been demonstrated previously, and the flexible 3D capabilities of the glass photonics platform are highlighted by a 1x4 splitter [20] and a 3x3 coupler [21].

4.1.2. Bragg gratings

The integration of Bragg gratings aids the miniaturization of sensing systems and strongly increases the application fields of integrated glass circuits. The two most commonly used techniques are point-by-point and modulation writing [22, Chapter 9]. In the former case, the Bragg grating is formed by individual voxel, each created by a single laser pulse. This is typically used with laser with a low repetition rate, and high pulse energies. Using this method, only higher order gratings can be created. For the modulation writing technique, an external modulation is superposed on the laser pulse train. The temporal modulation translates to a refractive index modulation during the writing, as such forming a Bragg grating. Our system employs a high-repetition rate laser, thus the latter technique is employed. The duty cycle was fixed to be 60 %, as previous studies showed this is the optimal duty cycle [10]. The optimal pulse energy was determined by the highest reflectivity obtained from the Bragg grating, and was found to be 310 nJ, which corresponds to the pulse energy for realizing the waveguides. An example Bragg grating spectrum for reflection and transmission is displayed in Figure 3. The 20 mm long Bragg grating was fabricated with a pulse repetition rate of 500 kHz, an external modulation frequency of 500 Hz, pulse energy of 310 nJ and a translation speed of 0.268 mm s^{-1}, as described in the section 3.

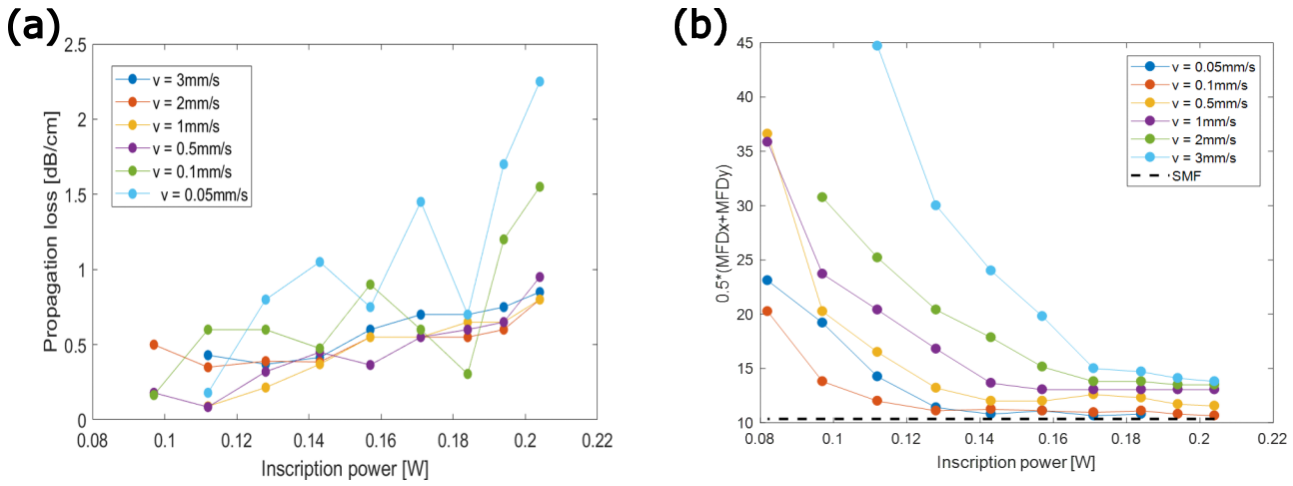

Figure 2: Waveguide characteristics for (a) propagation loss and (b) mode field diameter as a function of inscription power, with a pulse repetition rate of 500 kHz, for different translation speeds.

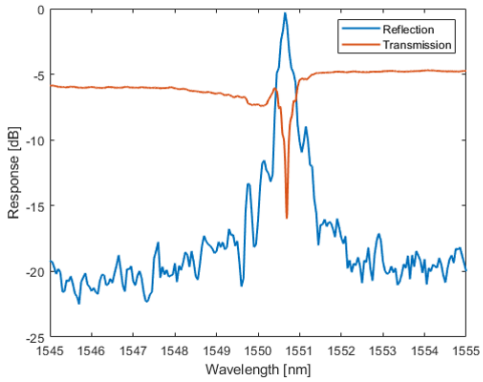

Figure 3: Bragg grating spectrum in reflection and transmission for a Bragg grating with target Bragg wavelength 1550 nm

4.1.3. *Microchannels and V-grooves for passive fiber alignment*

The most common structures fabricated using FLICE are microchannels. They can be used in a variety of applications mostly with the aim of microfluidics [14, 23, 15]; but they can also be used for optical switching, as has been demonstrated in our previous research [24].

Another application where the micrometer-level precision of FLICE (see section 3) is exploited is for the creation of V-grooves. In order for the integrated glass circuit to operate, it requires interfacing with light sources and detectors. Since integration of these directly on glass is less advanced, the currently mostly adopted approach is to (actively) align a butt-coupled fiber (array) to the glass chip and fixate it using adhesive. This is a time-consuming and costly procedure, often with a mechanically fragile connection. To facilitate packaging, V-grooves have been demonstrated by lasering the contour of the wanted V-groove and submerging the sample in KOH to selectively etch the laser exposed glass and lift out the bulk of the V-groove. A microscope image of a V-groove array is displayed in Figure 4. Special attention is paid on the end face of the groove. The laser parameters (200 nJ, 1 mm s^{-1}) are chosen to have a smooth end face to minimize coupling losses due to scattering. Etching of the V-groove was performed in a single etch step of 4 h. A coupling loss of around 1 dB was measured. V-grooves strongly facilitate packaging of glass chips as connection to a standard single mode fiber is required [25, 26]. This allows passive alignment, and a good mechanical stability of the fiber in the V-groove.

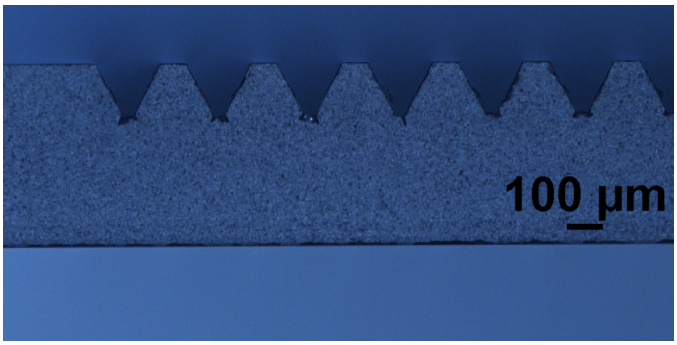

Figure 4: Microscope image of a V-groove array.

4.1.4. *Free-standing microstructures*

Using the same FLICE technology, freestanding structures can be created by etching completely through the glass, or underetching structures. This is, however, scarcely studied and reported in literature, especially when it comes to underetching. The creation of free-standing structures enables a new spectrum of possibilities and applications. Suspended waveguides have been demonstrated for their usage in vibration sensing [27]. In combination with microchannels, suspended Bragg gratings can be used to increase the sensitivity of the refractive index sensor, as for example designed in [23].

A specific type of freestanding structure that can be created within the glass photonics platform is a cantilever. Similar as for the suspended waveguide, this can be created by etching completely through the glass. This significantly decreased the

Table 1: Overview of laser parameters for different building blocks.

	pulse energy	writing speed	polarization (relative to writing direction)	modulation frequency
Waveguide (1550 nm)	310 nJ	0.5 mm s^{-1}	parallel	/
Bragg grating (1550 nm)	310 nJ	0.268 mm s^{-1}	parallel	500 Hz
V-groove	100-200 nJ	1-10 mm s^{-1}	parallel and orthogonal	/
Cantilever	200 nJ	1-10 mm s^{-1}	circular	/

required etching time, as the etchant can etch the structure from two sides. Creating a cantilever by underetching has proven to be more challenging. Firstly, there is limited access for the etchant to go underneath the structure and make it free-standing. This required more etching time. Because of the same limited access, it is harder to refresh the etchant underneath the structure, causing it to be depleted more rapidly. Hence, the underetching of the cantilever is the most time-consuming part of the process flow. To minimize the etching time, the cantilever was kept short and narrow, and a particular lasing strategy was employed. During the optimization it was observed that etching along the writing direction of the laser lines was faster than the etching in between adjacent laser lines. Therefore, stacked laser lines were written both along and orthogonal to the length of the cantilever, with a pitch of 4 µm between the laser lines in each direction. This strategy strongly decreases the etching time (to 3×4 h), while not significantly increasing the lasing time. Another method to overcome the extended etching time is to alter the shape of the cantilever. For example, when using a V-shape, the etchant can more easily underetch the cantilever.

One of the main concerns during fabrication of mechanical structures is that they are well-defined without causing excessive internal stress. During the inscription process, stress is built up due to the laser modification in the glass [28]. This stress is released during etching and can cause cracks in the substrate. These cracks are unwanted as they weaken the glass, lowering the strain it can be exposed to before failure. This is more rapidly expressed in cantilevers that have a rectangular shape, which resulted in cracks at the corners (see Figure 5). To minimize the local stress concentrations at the corners, the ends of the cantilever were rounded, as can be seen in Figure 5. At the fixed end of the cantilever, the radius of curvature is about 20 µm, while on the free end, the inner radius is 70 µm and the outer radius is 115 µm. The rounded corners had the desired effect and eliminated cracks.

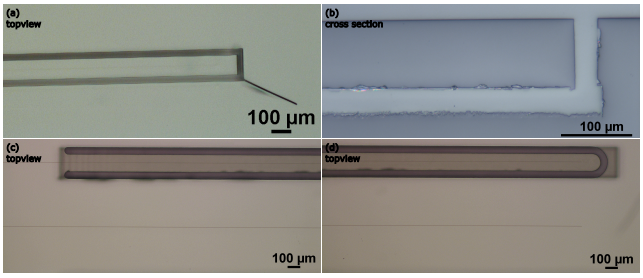

Figure 5: Microscope pictures of the cantilever. (a) cracks appearing at sharp corners, (b) cross-sectional view along the length at the free end of the cantilever, (c) top view of the fixec end of the cantilever, and (d) top view of the free end of the cantilever.

4.2. Overview

The table below provides an overview of the different building blocks, together with fabrication parameters used. All building blocks have a fixed pulse repetition rate of 500 kHz and a pulse width < 400 fs.

4.3. Temperature compensated strain sensor

To demonstrate the capabilities of the platform (monolithic combination of glass-based optical and micromechanical structures), a demonstrator is built composed of several of the above described building blocks. It is chosen to fabricate and charaterize a temperature compensated strain sensor. The general concept of the sensor relies on two Bragg gratings, of which one is mechanically isolated from the bulk of the substrate. This isolation is realized by the creation of a cantilever wherein one Bragg grating is integrated. When the sensor is strained in the direction along the Bragg gratings, the Bragg wavelength of the non-isolated Bragg grating will shift as a response to the applied strain. The isolated Bragg grating, on the other hand, will not experience strain. Hence, the Bragg wavelength will remain unchanged. The influence of temperature changes, on the other hand, is nearly identical for both Bragg gratings. In summary, the isolated Bragg grating is only sensitive to temperature, while the other is sensitive to both temperature and strain. Because of this, the parasitic influence of temperature present in the non-isolated Bragg grating, can be compensated by taking into account the response of the isolated Bragg grating.

4.3.1. Design

As illustrated in Figure 6, this concept can be realized using different designs and building blocks. All designs share a V-groove used for passive alignment of an optical fiber, for coupling light into the circuit. The first configuration utilizes a splitter to guide the light to the two Bragg gratings. In the depicted design, the Bragg gratings are located in-plane next to each other, however, the non-isolated Bragg grating can be positioned elsewhere, such as underneath the cantilever. The second configuration displays a so called in-line configuration, where the two Bragg gratings are consecutive in a single waveguide. This configuration can be implemented without a splitter, reducing the losses. However, an in-line configuration lengthens the sensor, and complicates temperature compensation as the two Bragg grating sensors are spaced further apart. A last configuration is to use two separate waveguides with V-grooves. Likewise to the previous configuration this reduces the sensor length as well as minimizes the losses of the circuit. The latter configuration is employed to demonstrate the platform and proof the concept of the temperature compensated strain sensor.

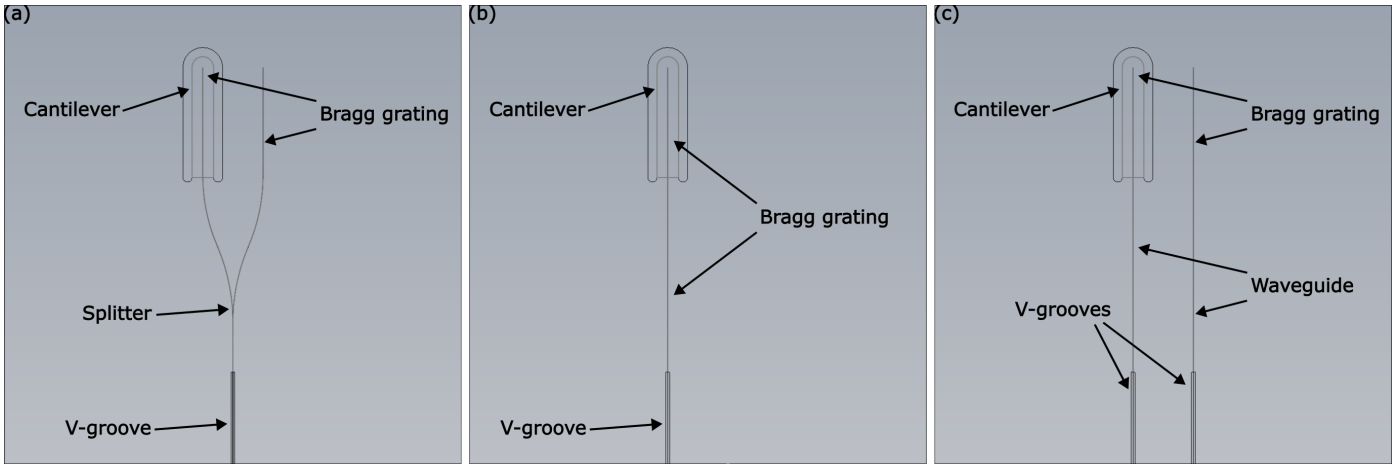

Figure 6: Different configurations to create a temperature compensated strain sensor with the different building blocks annotated.

4.3.2. *Thermal behaviour*

The thermal characteristics of the sensor were investigated by using a climate chamber and K-type thermocouple as reference sensor. As can be concluded from the transfer function depicted in Figure 7, the experimentally measured sensitivities of both Bragg gratings to temperature changes are virtually identical, with a value of about 10.5 pm $^{\circ}C^{-1}$, which corresponds to thermal sensitivities reported in literature [29]. Apart from the small difference, which can be accounted to the different wavelength of the Bragg gratings and measurement inaccuracies, the Bragg gratings behave as expected from the concept.

4.3.3. *Behaviour when strained*

For the tensile test, the sensor was bonded onto an aluminum plate using epoxy glue. The influence of the position of the epoxy on the strain transfer from the aluminum plate to the glass sensor has been studied with the help of numerical simulations. Detailed information on this can be found in the supplementary information.

Figure 7 shows the results of a tensile test performed on the designed sensor. The shift of Bragg wavelength of both Bragg gratings are depicted as function of the strain on the sensor (which was measured with a strain gauge glued onto the sensor as a reference). On the recorded Bragg grating reflection spectra a center of gravity (COG) fitting is performed for more accurate peak detection. The found sensitivity of the non-isolated Bragg grating is 1.1 pm/$\mu\epsilon$, which is close to the theoretical expectation of 1.23 pm/$\mu\epsilon$ [29]. The small difference can be accounted to imperfect placement of the strain gauge which was used as a reference sensor as well as potential inaccuracies of the measurement process. The isolated Bragg grating is proven to be insensitive to strain. Consequently, compensation of the parasitic thermal influences can be achieved.

5. Conclusion

A platform for fast prototyping and integrated glass optomechanical components is described based on femtosecond laser micromachining. This technology enables the fabrication of waveguides and Bragg gratings in glass substrates. On top of this, utilizing the femtosecond laser irradiation followed by chemical etching technology, free-standing, MOEMS-like structures can be created in glass with high aspect ratios. This is demonstrated by fabricating a temperature compensated strain sensor. The designed sensor substrate consists of two Bragg grating of which one is mechanically isolated from the rest of the substrate by the creation of an underetched cantilever. Strain measurements proved that the Bragg grating in the bulk of the glass is sensitive to strain with a sensitivity of 1.1 pm/$\mu\epsilon$, while the isolated Bragg grating in the cantilever does not experience any influence of strain. During temperature changes, both Bragg gratings exhibit a nearly identical sensitivity of 10.5 pm $^{\circ}C^{-1}$. Hence, temperature compensation can be easily performed. This platform allows transforming silica fiber based discrete optical functionality into a monolithic glass realization and allows realizing freestanding high aspect ratio 3D micromechanical structures and as such has the potential to realize opto-mechanical systems in glass.

Acknowledgment

The authors thank Grzegorz Gruca (Optics11) for the fruitful discussions and ideas.

References

[1] C. R. Doerr, K. Okamoto, Advances in silica planar lightwave circuits, Journal of Lightwave Technology 24 (12) (2006) 4763–4789. doi:10.1109/JLT.2006.885255.

[2] M. Merklein, B. Stiller, K. Vu, S. Madden, B. Eggleton, A chip-integrated coherent photonic-phononic memory, Nature Communications 8 (09 2017). doi:10.1038/s41467-017-00717-y.

[3] S. Nocentini, F. Riboli, M. Burresi, D. Martella, C. Parmeggiani, D. Wiersma, Three-dimensional photonic circuits in rigid and soft polymers tunable by light, ACS Photonics 5 (07 2018). doi:10.1021/acsphotonics.8b00461.

[4] L. Cerami, E. Mazur, S. Nolte, C. B. Schaffer, Femtosecond Laser Micromachining, Springer International Publishing, Heidelberg, 2013, pp. 287–321. doi:10.1007/978-3-319-00017-6_12.
URL https://doi.org/10.1007/978-3-319-00017-6_12

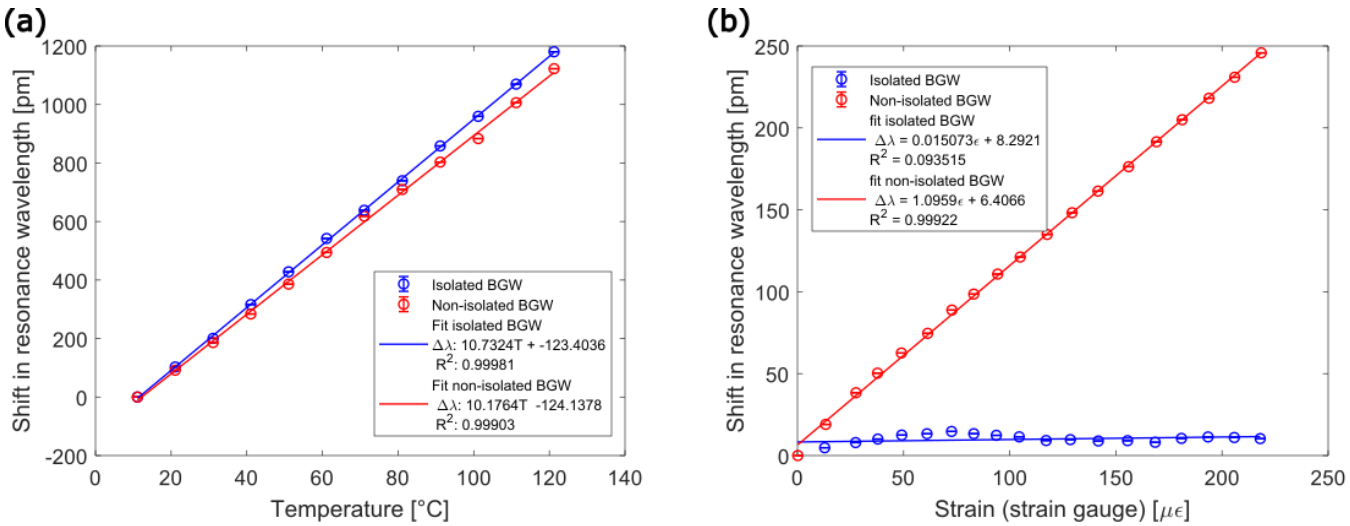

Figure 7: (a) Thermal and (b) strain response of the Bragg grating waveguides. Thermally they exhibit near identical behaviour, while only the non-isolated Bragg grating is sensitive to strain.

[5] K. M. Davis, K. Miura, N. Sugimoto, K. Hirao, Writing waveguides in glass with a femtosecond laser, Opt. Lett. 21 (21) (1996) 1729–1731. doi:10.1364/OL.21.001729.

[6] H. Wei, S. Krishnaswamy, Direct laser writing of a phase-shifted bragg grating waveguide for ultrasound detection, Opt. Lett. 44 (15) (2019) 3817–3820. doi:10.1364/OL.44.003817.

[7] J. R. Grenier, L. A. Fernandes, J. S. Aitchison, P. V. S. Marques, P. R. Herman, Femtosecond laser fabrication of phase-shifted bragg grating waveguides in fused silica, Opt. Lett. 37 (12) (2012) 2289–2291. doi:10.1364/OL.37.002289.

[8] H. Zhang, P. R. Herman, Chirped bragg grating waveguides directly written inside fused silica glass with an externally modulated ultrashort fiber laser, IEEE Photonics Technology Letters 21 (5) (2009) 277–279. doi:10.1109/LPT.2008.2010717.

[9] H. Zhang, S. Ho, S. Eaton, J. Li, P. Herman, Three-dimensional optical sensing network written in fused silica glass with femtosecond laser, Optics express 16 (2008) 14015–23. doi:10.1364/OE.16.014015.

[10] H. Zhang, S. Eaton, P. Herman, Single-step writing of bragg grating waveguides in fused silica with an externally modulated femtosecond fiber laser, Optics letters 32 (2007) 2559–61. doi:10.1364/OL.32.002559.

[11] P. Zeil, C. Voigtländer, J. Thomas, D. Richter, S. Nolte, Femtosecond laser-induced apodized bragg grating waveguides, Opt. Lett. 38 (13) (2013) 2354–2356. doi:10.1364/OL.38.002354.

[12] L. Borasi, E. Casamenti, R. Charvet, C. Dénéréaz, S. Pollonghini, L. Deillon, T. Yang, F. Ebrahim, A. Mortensen, Y. Bellouard, 3d metal freeform micromanufacturing, Journal of Manufacturing Processes 68 (2021) 867–876. doi:https://doi.org/10.1016/j.jmapro.2021.06.002.

[13] E. Casamenti, S. Pollonghini, Y. Bellouard, Few pulses femtosecond laser exposure for high efficiency 3d glass micromachining, Opt. Express 29 (22) (2021) 35054–35066. doi:10.1364/OE.435163.

[14] Y. Bellouard, A. Said, M. Dugan, P. Bado, Fabrication of high-aspect ratio, micro-fluidic channels and tunnels using femtosecond laser pulses and chemical etching, Opt. Express 12 (10) (2004) 2120–2129. doi:10.1364/OPEX.12.002120.

[15] S. LoTurco, R. Osellame, R. Ramponi, K. C. Vishnubhatla, Hybrid chemical etching of femtosecond laser irradiated structures for engineered microfluidic devices, Journal of Micromechanics and Microengineering 23 (8) (2013) 085002. doi:10.1088/0960-1317/23/8/085002.
URL https://dx.doi.org/10.1088/0960-1317/23/8/085002

[16] D. Ganziy, O. Jespersen, G. Woyessa, B. Rose, O. Bang, Dynamic gate algorithm for multimode fiber bragg grating sensor systems, Appl. Opt. 54 (18) (2015) 5657–5661. doi:10.1364/AO.54.005657.

[17] N. Mangal, B. Snyder, J. Van Campenhout, G. Van Steenberge, J. Missinne, Expanded-beam backside coupling interface for alignment-tolerant packaging of silicon photonics, IEEE Journal of Selected Topics in Quantum Electronics 26 (2) (2020) 1–7. doi:10.1109/JSTQE.2019.2934161.

[18] V. A. Amorim, J. M. Maia, D. Alexandre, P. V. S. Marques, Optimization of broadband y-junction splitters in fused silica by femtosecond laser writing, IEEE Photonics Technology Letters 29 (7) (2017) 619–622. doi:10.1109/LPT.2017.2675858.

[19] W.-J. Chen, S. M. Eaton, H. Zhang, P. R. Herman, Broadband directional couplers fabricated in bulk glass with high repetition rate femtosecond laser pulses, Opt. Express 16 (15) (2008) 11470–11480. doi:10.1364/OE.16.011470.

[20] W.-H. Yuan, J.-M. Lv, X.-T. Hao, F. Chen, Optimization of waveguide structures for beam splitters fabricated in fused silica by direct femtosecond-laser inscription, Optics & Laser Technology 74 (2015) 60–64. doi:https://doi.org/10.1016/j.optlastec.2015.05.016.

[21] K. Suzuki, V. Sharma, J. G. Fujimoto, E. P. Ippen, Y. Nasu, Characterization of symmetric 3x3 directional couplers fabricated by direct writing with a femtosecond laser oscillator, Opt. Express 14 (6) (2006) 2335–2343. doi:10.1364/OE.14.002335.

[22] R. Osellame, G. Cerullo, R. Ramponi, Femtosecond Laser Micromachining: Photonic and Microfluidic Devices in Transparent Materials, Topics in Applied Physics, Springer Berlin Heidelberg, 2012.
URL https://books.google.be/books?id=WDykKnqoD1IC

[23] V. Maselli, J. R. Grenier, S. Ho, P. R. Herman, Femtosecond laser written optofluidic sensor: Bragg grating waveguide evanescent probing of microfluidic channel, Opt. Express 17 (14) (2009) 11719–11729. doi:10.1364/OE.17.011719.

[24] A. Radosavljević, A. Desmet, J. Missinne, K. Saurav, V. Panapakkam, S. Tuccio, C. L. Arce, J. Watté, D. Van Thourhout, G. Van Steenberge, Femtosecond laser-inscribed non-volatile integrated optical switch in fused silica based on microfluidics-controlled total internal reflection, Journal of Lightwave Technology 38 (15) (2020) 3965–3973. doi:10.1109/JLT.2020.2983109.

[25] Desmet, Andres and Radosavljevic, Ana and Missinne, Jeroen and Van Thourhout, Dries and Van Steenberge, Geert, Laser written glass interposer for fiber coupling to silicon photonic integrated circuits, IEEE PHOTONICS JOURNAL 13 (1) (2021) 13.
URL http://dx.doi.org/10.1109/jphot.2020.3039900

[26] Geudens, Viktor and Van Steenberge, Geert and Missinne, Jeroen, Femtosecond laser written Bragg grating sensors with passive fiber alignment structures in fused silica (2021).
URL http://dx.doi.org/10.1109/IPC48725.2021.9593075

[27] E. Casamenti, T. Yang, P. Vlugter, Y. Bellouard, Vibration monitoring based on optical sensing of mechanical nonlinearities in glass suspended waveguides, Opt. Express 29 (7) (2021) 10853–10862. doi:10.1364/OE.414191.

[28] Y. Bellouard, A. Champion, B. McMillen, S. Mukherjee, R. Thomson,

C. Pépin, P. Gillet, Y. Cheng, Stress-state manipulation in fused silica via femtosecond laser irradiation, Optica 3 (12) (2016) 1285–1293. doi:10.1364/OPTICA.3.001285.

[29] H. Zhang, S. Ho, S. M. Eaton, J. Li, P. R. Herman, Three-dimensional optical sensing network written in fused silica glass with femtosecond laser, Opt. Express 16 (18) (2008) 14015–14023. doi:10.1364/OE.16.014015.